# The role of fluctuations and stress on the effective viscosity of cell aggregates

Philippe Marmottant[a,1], Abbas Mgharbel[b,1], Jos Käfer[a], Benjamin Audren[b], Jean-Paul Rieu[b], Jean-Claude Vial[a], Boudewijn van der Sanden[c], Athanasius F. M. Marée[d], François Graner[a,e], and Hélène Delanoë-Ayari[b,2]

[a]Laboratoire de Spectrométrie Physique, Unité Mixte de Recherche 5588, Université Grenoble I and Centre National de la Recherche Scientifique, 140 Avenue de la Physique, F-38402 Martin d'Hères Cedex, France; [b]Laboratoire Matériaux et Phénomènes Quantiques, Centre National de la Recherche Scientifique, Unité Mixte de Recherche 5586, Université de Lyon, Université Lyon 1, 43 Boulevard du 11 novembre 1918, F-69622 Villeurbanne Cedex, France; [c]Institut des Neurosciences Grenoble, Institute National de la Santé et de la Recherche Médicale U836, Chemin Fortuné Ferrini, BP 170, F-38042 Grenoble Cedex 9, France; [d]Theoretical Biology/Bioinformatics, Utrecht University, Padualaan 8, 3584 CH Utrecht, The Netherlands; and [e]Biologie du Développement, Unité Mixte de Recherche 3215 Institut Curie and Centre National de la Recherche Scientifique, Institut National de la Santé et de la Recherche Médicale U934, 26 Rue d'Ulm, F-75248 Paris Cedex 05, France

**Cell aggregates are a tool for in vitro studies of morphogenesis, cancer invasion, and tissue engineering. They respond to mechanical forces as a complex rather than simple liquid. To change an aggregate's shape, cells have to overcome energy barriers. If cell shape fluctuations are active enough, the aggregate spontaneously relaxes stresses ("fluctuation-induced flow"). If not, changing the aggregate's shape requires a sufficiently large applied stress ("stress-induced flow"). To capture this distinction, we develop a mechanical model of aggregates based on their cellular structure. At stress lower than a characteristic stress $\tau*$, the aggregate as a whole flows with an apparent viscosity $\eta*$, and at higher stress it is a shear-thinning fluid. An increasing cell–cell tension results in a higher $\eta*$ (and thus a slower stress relaxation time $t_c$). Our constitutive equation fits experiments of aggregate shape relaxation after compression or decompression in which irreversibility can be measured; we find $t_c$ of the order of 5 h for F9 cell lines. Predictions also match numerical simulations of cell geometry and fluctuations. We discuss the deviations from liquid behavior, the possible overestimation of surface tension in parallel-plate compression measurements, and the role of measurement duration.**

cellular Potts model | statistical model | surface tension



**Fig. 1.** Shape of aggregates. (*A*) Top view, two-photon microscopy image of the middle plane of a F9 aggregate at a 27% compression rate between parallel plates (see also Fig. S1). (Scale bar, 50 $\mu$m.) Cells are alive and moving (*SI Text* and Movie S1). (*B*) Side view, in a stereomicroscope (*SI Text*). (Scale bar, 125 $\mu$m.) (*C*) Simulation of three successive compressions.

Cell aggregates (1) (Fig. 1 *A* and *B*), also called multicellular spheroids, are made of either a single cell type, or mixtures of different types; for a review, see refs. 2 and 3. They have become a classical tool for studies on morphogenesis (4), cancer invasion, and tissue engineering (2).

One century ago, it was discovered that two different cell types, when mixed, can sort out (5), like several two-phase physical systems do to minimize energy. Such cell sorting can be interpreted through cell adhesion differences: Motile cells rearrange to minimize the overall energy of the aggregate (6). By compressing an aggregate between two parallel plates (7), measuring its pressure and curvatures determines its surface tension (assuming that Laplace's law holds) (3, 7, 8). Comparing the surface tension values obtained for different cell types enables one to predict their sorting behavior (9). Thus, equilibrium configurations of aggregates display analogies with the shape of liquid drops (4).

When put in contact, two aggregates can fuse, and the resulting aggregate rounds up (10, 11) (Movie S2), yielding quantitative measurements of an effective aggregate viscosity (*SI Text* and Fig. S2) (12). Hence even out of mechanical equilibrium, aggregates have analogies with liquids: More precisely, they flow like complex (non-Newtonian) fluids (13–15). Their behavior depends on the time scale and duration of the measurement. For instance, Leghorn embryo cell aggregates subjected to brief centrifugation periods (8–16 min) flatten quickly (cell shapes flatten too), and round up quickly (in <2 min) once centrifugal forces are removed, reaching a shape very
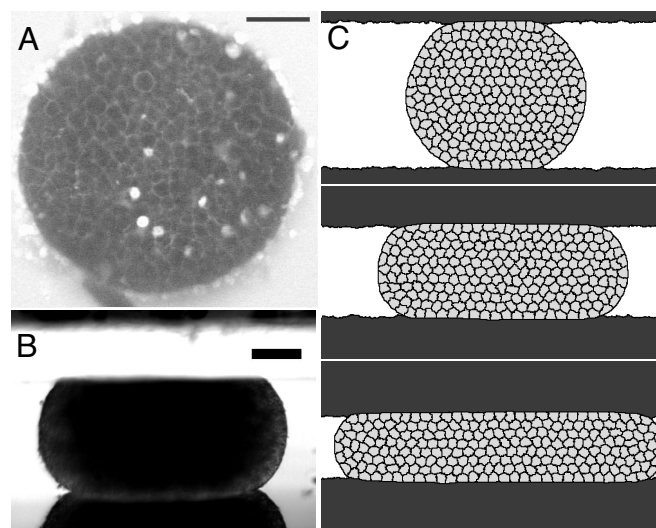
similar to the initial one, like an elastic solid (16). In contrast, during prolonged centrifugation (1 day), the same aggregates continue to flatten more slowly (while cells gradually reassume their original shapes) (17, 18); once centrifugal forces are removed, these aggregates round up slowly (in ≈1 d), like a viscous liquid.

Existing models usually involve a phenomenological viscoelastic description (13, 15–17). However, aggregates are space-filling assemblies of deformable cells and thus belong to the class of biological or physical cellular materials (19) like liquid foams (20). As such, they can display viscous, elastic, and plastic behaviors (21). Here, we develop a model based on their cellular structure that captures the complexity of their triple mechanical
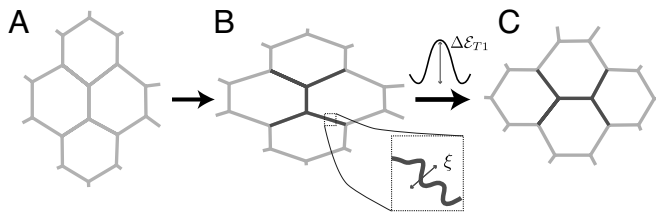
**Fig. 2.** A neighbor swapping ["T1" topological rearrangement (20)]. (*A*) Sketch of initially relaxed cells. (*B*) Flattened cells, with a deformation $\varepsilon_{cell}$ due to stress. (*Inset*) (*Upper*) Energy barrier $\Delta\varepsilon_{T1}$ to overcome for a T1 to occur. (*Inset*) (*Lower*) Membrane fluctuations with amplitude proportional to $\xi$. (*C*) After a T1: The cell arrangement has changed, and the cell shapes relax, dissipating energy.

behavior. We compare its predictions with large-amplitude compression experiments (Fig. 1 *A* and *B*) and corresponding simulations (Fig. 1*C*). With two-photon microscopy, we image in situ cell shapes (Fig. 1*A* and Fig. S1), cell shape changes, and rearrangements (Movie S1).

## Model

**Global Description of the Aggregate.** At a scale much larger than the cell size, the aggregate can be characterized by its state of deformation and stress ("continuous medium" description).

In a parallel-plate compression experiment, we quantify the aggregate deformation by its relative height change, $\varepsilon_{tot} = (h_{ag} - h)/h_{ag}$. Here, $h_{ag}$ is the aggregate's initial height (i.e., diameter), corresponding to the plate separation at the time of first contact; $h$ is its current height ($h < h_{ag}$). During compression, $h$ is equal to the current plate separation $h_{comp}$; during free decompression $h$ increases.

The force exerted by the aggregate on the plates is the cross-section area $S$ of the aggregate through its midplane times the internal stress of the compressed aggregate (see *SI Text* for the tensorial description):

$$F_{plate} = (p + \tau)S. \qquad [1]$$

Here, $p$ is the hydrostatic pressure and $\tau$ the elastic contribution to the stress, which we study here. In the case of a drop made of a simple liquid ($\tau = 0$) with surface tension $\sigma$, at equilibrium, $p$ would be balanced by the drop mean curvature $\kappa$ [Laplace law: $p = \sigma\kappa$ (8)].

**Local Description at the Cell Level.** We assume the cell deformation (monitored by the relative cell size change, $\varepsilon_{cell}$) and the stress are small enough to be proportional:

$$\tau = E\varepsilon_{cell}, \qquad [2]$$

where $E$ is a stiffness (elastic modulus).

Within aggregates of inert objects such as drops (emulsions) or bubbles (foams), a "T1" (20) occurs when the local stress is high enough to overcome the energy barrier, $\Delta\varepsilon_{T1}$ (Fig. 2), which depends on the interfaces' tension and length. It marks the transition from a reversible (elastic) object shape change to an irreversible (plastic) rearrangement, after which energy is dissipated (21). The energy barriers are biased and easier to overcome in the direction of the stress (21): Rearrangements accumulate and result in a continuously increasing material deformation, noted $\varepsilon_{rea}$, analogous to a flow. Because $\varepsilon_{rea}$ does not correlate with each object's individual deformation, it has no direct elastic contribution to stress (and we neglect the contribution to the stress arising from each object's internal viscosity).

Unlike inert objects, living cells overcome some energy barriers, with large membrane shape fluctuations (Movie S1). These

fluctuations are active and associated with cytoskeleton dynamics, as is evidenced by studies on cells treated with cytochalasin-B (an actin depolymerizing drug) (22, 23). An effective temperature or, equivalently, a thermal energy scale $\xi$ (also noted $kT$ in the literature) (23), describes not only the amplitude of these interface fluctuations (23, 24) but also the diffusion of a cell throughout an aggregate (25).

**Mechanical Behavior of the Aggregate.** To capture the main physical ingredients that determine the aggregate's liquid behavior, we simplify its description. We consider here that all energy barriers have the same height, that of a T1. We take the total deformation to be:

$$\varepsilon_{tot} = \varepsilon_{cell} + \varepsilon_{rea}. \qquad [3]$$

In the absence of stress, fluctuation-induced rearrangements switch back and forth, with no flow on average. According to the Eyring model (26), the probability of rearrangement in the direction of stress (i.e., a T1 that reduces stress) is favorable: $f^+ = f\exp\{(-\Delta\varepsilon_{T1} + \tau V\delta\varepsilon)/\xi\}$. Here, $f$ is the inverse of a time ("attempt frequency"): It is a phenomenological quantity that characterizes how often fluctuations occur, only a fraction of which are actually able to jump over energy barriers; $\tau V$ is the work gained during a rearrangement in the direction favored by the stress ($V$ is of the order of a cell volume) and $\delta\varepsilon$ the deformation associated with a rearrangement.

In the direction opposing stress, the probability of a rearrangement is less favorable: $f^- = f\exp\{(-\Delta\varepsilon_{T1} - \tau V\delta\varepsilon)/\xi\}$. The flow rate $\dot{\varepsilon}_{rea}$ results from the difference between favored and unfavored rearrangement probabilities:

$$\dot{\varepsilon}_{rea} = (f^+ - f^-)\delta\varepsilon = \frac{\tau^*}{\eta^*}\sinh\left(\frac{\tau}{\tau^*}\right). \qquad [4]$$

Here, both $\tau^*$ and $\eta^*$ are continuous medium parameters (related to cell properties, see *Discussion*). The characteristic stress $\tau^* = \xi/V\delta\varepsilon$ is determined by the fluctuation amplitude and cell size. The characteristic viscosity $\eta^* = \xi\exp(\Delta\varepsilon_{T1}/\xi)/2fV\delta\varepsilon^2$ depends on $\tau^*$ and energy barriers (but not on the internal viscoelasticity of cells).

**Two Regimes.** Eq. **4** relates the aggregate's deformation and the applied stress; together with Eqs. **2** and **3**, it fully describes the aggregate's mechanical response, i.e., the time evolution of the flow for any given configuration ("constitutive equation"). The characteristic stress $\tau^*$ separates two regimes: that of fluctuation- and stress-induced flows.

If the stress $\tau$ is much smaller than $\tau^*$, the flow is due to fluctuations. The viscous stress and the flow rate are proportional to each other, $\tau \simeq \eta^*\dot{\varepsilon}_{rea}$ (Eq. **4**). The associated time scale over which stress disappears is: $t_c = \eta^*/E \sim \exp\{\Delta\varepsilon_{T1}/\xi\}$. If $t_c$ is smaller than or comparable with the duration of the measurement, at large scale, the aggregate relaxes the stress like a simple (Newtonian) fluid of viscosity $\eta^*$ (Fig. S2). Conversely, if $t_c$ is much larger than the duration of the measurement, the flow is not measurable, and the aggregate seems to display a solid (plastic) behavior.

In contrast, if the stress $\tau$ is larger than $\tau^*$, it overcomes energy barriers. According to Eq. **4**, the ratio of the viscous stress to the flow rate defines an effective viscosity $\eta_{eff}$, that is smaller than $\eta^*$, by a factor $\eta_{eff}/\eta^* = (\tau/\tau^*)/\sinh(\tau/\tau^*)$. The aggregate thus behaves like a "shear-thinning" fluid in which viscosity decreases at higher $\tau$.

**Compressions: Predictions.** Eq. **4** applies to compressions or decompressions. In a compression (Fig. 1), the distance $h$ between plates is decreased in a stepwise manner, then is kept constant
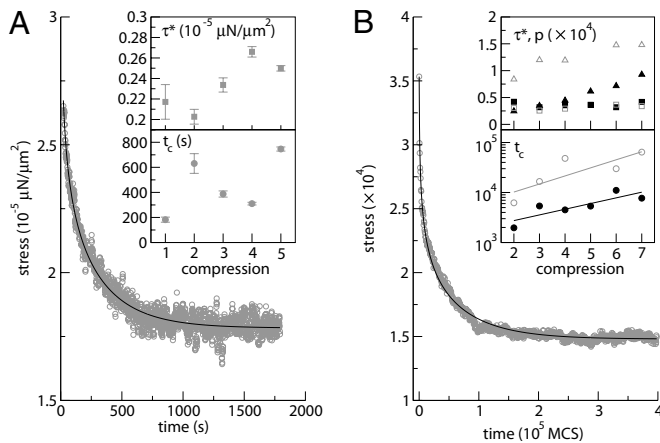
**Fig. 3.** Stress relaxation while the compression plate is quickly displaced then kept fixed (constant distance $h$: "step-strain"). (*A*) Experiments showing the immediate force relaxation of an aggregate (initial diameter 500 $\mu$m) for the first compression. Gray circles, measured stress; solid line, fit from Eqs. **1** and **5** after subtraction of the asymptotic plateau value $p$ (3). (*Inset*) Characteristic stress $\tau^*$ and stress relaxation time $t_c$ fitted to five ($n = 1–5$) successive compressions. (*B*) Simulations of long-term cell rearrangements. Gray circles, measured stress, here with $\gamma_{CC} = 6.78 \times 10^5$; solid line, fit from Eqs. **1** and **5**. (*Inset*) Fitted parameters for cell–cell tension $\gamma_{CC} = 1.13 \times 10^5$ (black filled symbols) or $6.78 \times 10^5$ (gray open symbols). Squares, $\tau^*$; circles: $t_c$; triangles, asymptotic plateau value $p$. The initial contact ($n = 1$) does not correspond to any measurable force. In the *Lower Inset* graph, note the log scale of the vertical axis; linear fits are drawn to guide the eye.

to $h = h_{comp}$, so that $\varepsilon_{tot} = \varepsilon_{comp}$, and $\dot{\varepsilon}_{tot} = 0$. This creates an initial elastic stress $\tau_0 = E\varepsilon_{comp}$. Eqs. **2–4** then yield a first-order differential equation. Its solution is the relaxation of stress with time $t$ (Fig. 3):

$$ \tau(t) = 2\tau^* \tanh^{-1}\left[ \tanh\left(\frac{\tau_0}{2\tau^*}\right) \exp\left(-\frac{t}{t_c}\right) \right]. \quad [5] $$

Initially, the flow is in the stress-induced regime: The stress decreases faster than $\exp(-t/t_c)$. When the stress reaches $\tau^*$, the flow enters the fluctuation-induced regime, where the stress decreases like $\exp(-t/t_c)$.

In principle, after a sufficiently long compression time ($t_{comp} \gg t_c$) all elastic stresses ultimately disappear (Eq. **5**). At this stage, the plates would only measure the constant contribution arising from the hydrostatic pressure generated by the aggregate surface tension. On the contrary, if $t_{comp}$ is smaller (or not much larger) than $t_c$, the aggregate still stores some residual stress, like a plastic solid.

## Experimental and Numerical Tests

**Compression Experiments.** When an aggregate is compressed between plates (Fig. 1 *A* and *B*), the stress is initially high then decreases (Fig. 3*A*). The shape of the relaxation curve is well fitted by our model. During successive compressions the characteristic stress remains approximately constant, $\tau^* \simeq 2.4$ Pa (Fig. 3*A* Inset). In the curve of Fig. 3*A*, the initial stress is 9 Pa above the asymptotic plateau value: $\tau_0/\tau^* \simeq 3.8$; hence, we estimate that initially $\eta_{eff}/\eta^* \simeq 0.2$. The characteristic time $t_c$ is of the order of a few $10^2$ s. To understand the small value of this time scale (which might be associated with cytoskeletal dynamics, see *Discussion*), in what follows we distinguish the contributions from subcellular and cell levels to the dynamics.

**Compression Simulations.** First, we simulate the collective cell behavior, i.e., the global flow, in a compressed aggregate (Fig. 1*C*) without subcellular structure. We only use cell-level ingre-

dients: cell shapes and rearrangements, internal pressure, cell–cell interface tension and fluctuations. The stress relaxation agrees with Eq. **5** (Fig. 3*B*).

At low cell–cell tension (closed symbols in Fig. 3*B* Inset), the asymptotic plateau value compares well to the measured static pressure, $p = \sigma\kappa$, as in a simple liquid. As expected (since in the model it is mostly determined by the fluctuation amplitude) $\tau^*$ is constant through successive compressions of the same aggregate. The characteristic time $t_c$, which depends on $\Delta\mathcal{E}_{T1}$, strongly increases during successive compressions. This increase might be related to the existence of energy barriers with different values (see *Discussion*): Low energy barriers are passed first, higher barriers later.

Simulations with larger cell–cell tensions (open symbols in Fig. 3*B* Inset) yield a similar $\tau^*$ and a slower $t_c$ (larger viscosity), as expected. The deviation from the liquid behavior is larger (see also Fig. S4): The asymptotic plateau value is higher; hence, a residual elastic stress contaminates the measurements of hydrostatic pressure (see *Discussion*).

**Compression–Decompression Cycle Experiments.** Second, we perform measurements at a much larger time scale, during free relaxation (see also fusion, *SI Text* and Fig. S2). An aggregate is compressed at a fixed height $h_{comp}$ (corresponding to a deformation $\varepsilon_{comp}$) during a time $t_{comp}$; then the upper plate is removed and the aggregate is left free (Fig. S3, Movie S3). The aggregate height relaxes quickly $\simeq 10^2$ s, then more slowly (Fig. S3).

In our model, during the compression time $t_{comp}$, rearrangements contribute to the aggregate flow, and a rearrangement deformation $\varepsilon_{rea}$ builds up (Eq. **4**). At the end of the compression, these rearrangements have relaxed the stress down to the value $\tau(t_{comp})$, predicted by Eq. **5**. The stored elastic deformation therefore decreases from $\varepsilon_{comp}$ to $\varepsilon_{cell} = \tau(t_{comp})/E$. Because the total deformation is kept constant, we have (Eq. **3**) $\varepsilon_{tot} = \varepsilon_{comp} = \varepsilon_{cell}(t_{comp}) + \varepsilon_{rea}$: The decrease in elastic deformation is exactly compensated by the rearrangement deformation. The arrangement of cells has been modified irreversibly. Upon removal of the compression plate, the aggregate surface tension drives rounding. At time scales shorter than hours $h$ does not come back to its original value $h_{ag}$. The residual deformation, equivalent to an apparent plasticity (see figure 5 of ref. 13) $\varepsilon_{plastic} = \varepsilon_{rea}$ is:

$$ \varepsilon_{plastic} = \varepsilon_{comp} - \frac{\tau(t_{comp})}{E}. \quad [6] $$

For several values of $\varepsilon_{comp}$ and $t_{comp}$, the model agrees (Fig. 4) with the experimental residual deformation. We measure it at a time long enough for internal elastic stresses to have relaxed: We fix it by convention here at 440 s (Fig. S3). The relaxation time is $t_c = 5$ h. The characteristic deformation is $\varepsilon^* = \tau^*/E = 0.13$: It means that the characteristic stress $\tau^*$ is reached if the aggregate is quickly compressed to an amplitude of at least 0.13.

## Discussion

**Energy Barriers and Nonreleased Elasticity.** Elasticity and plasticity arise from contributions of cell bulk (cytoskeleton and organelles) and surface (actomyosin-rich cortex). Adhesion and cortical contraction contribute to create a cell–cell interfacial tension [not to be confused with the aggregate surface tension (19, 27)] and, thus, energy barriers.

We study the combined effect of stress and active fluctuations to overcome energy barriers. Model and simulations suggest that higher interfacial tensions, by increasing the energy barriers, give rise to a higher viscosity. Our model captures the main features of compression experiments and simulations, as well as free relaxations, and distinguishes two flow regimes. Fits to the data (Fig. 3) determine $\tau^*$, $t_c$, and an asymptotic plateau value.
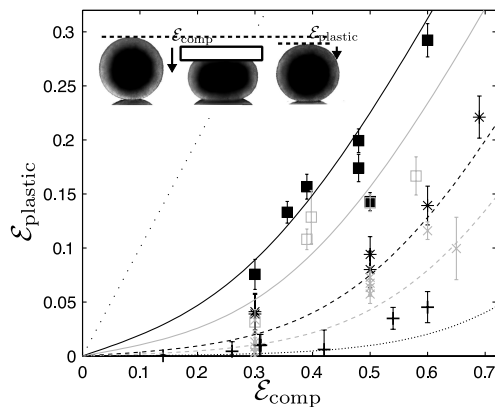
**Fig. 4.** Apparent plasticity. An aggregate is compressed at a fixed height $h_{comp}$ during a time $t_{comp}$ and then the upper plate is removed and the aggregate is left free to relax (Movie S3). We define and measure $h_p$ as the height $h$ measured by convention after 440 s (Fig. S3). Symbols indicate $t_{comp}$: black +, 1 min; gray ×, 5 min; black *, 10 min; gray open squares, 30 min; filled squares, 60 min. Lines: prediction of Eqs. **5** and **6** plotted with $t_c = 5$ h and $\tau^*/E = 0.13$; thin straight dotted line: prediction with $t_{comp} = \infty$, i.e., $\varepsilon_{plastic} = \varepsilon_{comp}$. (*Inset*) Images of aggregates before compression ($h_{ag}$), during compression ($h_{comp}$), and after decompression ($h_p$); $\varepsilon_{comp} = (h_{ag} - h_{comp})/h_{ag}$, $\varepsilon_{plastic} = (h_{ag} - h_p)/h_{ag}$.

To interpret the values of these parameters, it is necessary to take explicitly into account not only cell rearrangements, but also the subcellular (cytoskeleton) dynamics. If the model were also developed for cell internal reorganization, Eq. **5** would be well suited to fit both types of force relaxations. A future extension of our single energy barrier model might include a more realistic distribution of energy barriers, some of which can be passed by fluctuations, whereas others are not passed within the experiment duration.

**Time Scales.** The slow time scale $t_c = 5$ h (Fig. 4) can be interpreted as the relaxation time due to rearrangements, visible on Movie S1. Rearrangements-induced flow starts when aggregates are out of mechanical equilibrium, e.g., compressed. Rearrangements continue over hours until the complete equilibration of the aggregate. This interpretation agrees with the cell shape relaxation observed after 24 h in a centrifuged aggregate (16). It also agrees with orders of magnitude extracted from the fusion of two F9 aggregates and the rounding of the resulting aggregate, driven by surface tension, which takes 6 h (Fig. S2, Movie S2); we estimate $\eta^* = 4.4 \ 10^5$ Pa·s: Combined with the above relations $\tau^* = 0.13E$ and $E = \eta^*/t_c$ this yields $\tau^* = 3.2$ Pa, which is the same order of magnitude as in compression (Fig. 3*A Inset*).

We observe a much shorter time scale ($\approx 10^2$ s) in force relaxation experiments (Fig. 3*A*), confirmed by height recovery after compression (Fig. S3). We believe that it is due to internal release of cell elasticity, not included in the model nor in the simulations. It is compatible with the internal cell viscosity, probably hundreds of times smaller (28) than $\eta^*$.

Aggregates are not always able to fuse and round up within the time of experiments or simulations [CHO cell aggregates barely fuse even after 1 week (11)]. In addition, even after relaxation, their shape sometimes displays a strong deviation from that of a liquid drop (22, 23) (Fig. S4). This suggests that the energy barriers are too high: Both the aggregate's surface tension and the fluctuations are insufficient to relax the elastic stress over the duration of the experiment. Our simulations at high cell–cell tension (open symbols, Fig. 3*B Inset*; Fig. S4) confirm that a plateau is sometimes reached before full stress relaxation.

**Effect on Measured Surface Tension.** In compression–decompression cycle experiments, at a given relaxation time, the longer or the stronger the compression, the larger the number of rearrangements, and thus the stronger the apparent irreversibility, in good agreement with Eqs. **5** and **6**.

For the assessment of surface tension, the time between two successive compressions is usually between 30 min and 2 h (7, 11). An equilibrium force seems to be attained 2–10 min after compression. We believe that this time is large enough to relax internal contributions; but, unlike what is assumed by ref. 13, only a limited number of rearrangements have taken place. Residual elastic contributions could lead to an overestimation of surface tension. This questions the validity of the application of Laplace's law in past surface tension measurement experiments.

A likely hypothesis would explain the remaining stored elasticity in our experiments by an active response of the cell. When compressed, cells could actively release a part of the elasticity stored in the compressed cytoskeleton; when decompressed, the surface tension drives the relaxation of the global aggregate shape, and cells could actively regain part of the elasticity. This hypothesis is compatible with the rate, 1–10 $\mu$m/min, at which single cells reorganize their cytoskeleton (29). It could be tested by two-photon imaging of cell contours and simultaneous force measurements recording while modifying the dynamics of actin (using drugs such as latrunculin and jasplakinolide) microtubules, or intermediate filaments.

If this hypothesis is correct, the elastic energy stored in deformed cells will be less than we assume in our model and simulations, and the overestimation of the surface tension in compression experiments will be smaller. This will explain why published measurements of surface tension are usually robust and do not depend on compression magnitude and duration, nor on aggregate size (3, 7, 9, 13).

## Materials and Methods

**Cell Line and Aggregates Preparation.** Mouse embryonal carcinoma F9 cell line was a generous gift from A. Nagafuchi (Kumamoto University, Japan) (30). Cells were maintained in DMEM (41965-039; GIBCO) supplemented with 10% fetal bovine serum (2902 P-232310; Biotech GmbH). For the aggregate formation, cells were dissociated and reassembled in 15-$\mu$L hanging drops containing between 1,000 and 8,000 cells (3). After 2 days, the newly formed aggregates were transferred to cell culture plates (24 wells) containing fresh medium and then put on a gyratory shaker for two more days. For the compression measurements, the cell aggregates were transferred to $CO_2$-independent medium (18045-054; GIBCO).

**Compression–Decompression Experiments.** Each aggregate was compressed, by successive steps of 50 $\mu$m, between two glass plates. The lower one (2-mm-thick borosilicate glass) is located at the bottom of a $CO_2$-independent medium chamber that is moved in the x,y,z directions by a micromanipulator (MP285; Sutter Instrument). The upper one (cover glass) is fixed to a rigid pipe, except in Fig. 3*A*, that uses the force sensor described in ref. 3. The whole setup is embedded in a thermally isolated chamber maintained at the desired temperature by a resistance traversed by a current that is modulated by a temperature controller (331; Lakeshore). The chamber in which aggregates are deposited for the experiment is open to air to facilitate displacements and choice of aggregates; the free surface is covered with a thick mineral oil layer to prevent evaporation. Glass surfaces are carefully cleaned with soap and pure water (sonicated 30 min with 2% Microson detergent; Fisher Bioblock). They are made hydrophobic by silanization with perfluorosilane (F06179; ABCR) and covered with Pluronic F-127 (Sigma) at 10 mg/mL for 5 min and then rinsed briefly with water and dried. This treatment ensures that the aggregate adhesiveness remains small. For details see ref. 3 and *SI Text*.

In Fig. 3*A*, the error bar on fitted parameters is the 95% confidence interval of the nonlinear curve fit: All fitted parameters have errors <10% of the estimated value and smaller than the data dispersion. In Fig. 4, each error bar is estimated on only one aggregate decompression experiment as the uncertainty on the optical measurement of $h_{ag}$, $h_p$ and $h_{comp}$; it depends on image resolution and aggregate roughness as well as the possible slight aggregate rotation and translation after decompression.

**Two-Photon Microscopy.** Two-photon laser scanning microscopy is performed on an Olympus BX50WI microscope coupled to a Bio-Rad MRC 1024 scan head with a nondescanned detector to increase the observation depth. An 800-nm excitation beam from a Tsunami femtosecond Ti:Saphire laser (Millenia V; Spectra-Physics) is focused on the surface of the aggregate by using a magnification ×20 water-immersion objective (0.95 N.A., Xlum Plan Fl; Olympus). The beam scans the $xy$ plane to acquire $512 \times 512$-pixel images in 0.9 s. Variation of the observation depth ($z$-scan) is realized by moving the motorized objective vertically. We have developed a compression apparatus similar to that described in ref. 11 mounted on the stage of the two-photon microscope with a thermostatted circulating water bath to control temperature at 37 °C. The soluble dye sulforhodamine B (SRB), injected at a concentration of 8 $\mu$g/mL in the culture medium, quickly diffuses inside aggregates and stains the extracellular space with an intensity comparable with the SRB present outside of the aggregates.

**Cellular Potts Model Simulations.** The cellular Potts model (31, 32) is a standard algorithm to simulate multicellular structures (and cell packing) from individual cells of variable shape and size (32). Each cell is defined as a certain set of pixels, here in 2D [tests in 3D yielded similar results (33)]; their number defines the cell area $A$. The aggregate energy has two terms (31).

First, the interfacial energy between cells is the sum of the energy costs between pixels that form the border between different cells (all cells here are of the same type, noted C), as well as between one cell and the medium (M) or the plate (P). A pair of two pixels $i$ and $j$ at such a border has an associated energy cost $\gamma_{ij}$, with, here, the following combinations: $\gamma_{CC}$, $\gamma_{CM}$, $\gamma_{CP}$, or $\gamma_{MP}$. These are inputs of the simulations and are constant [making them variable (33) does not significantly change the results presented here]. We account for the proportionality factor between energy and perimeter, here 11.3 (33), due to the average number of pixel pairs included in the evaluation of energy.

Second, the elastic energy for each cell is the sum over cells of $\lambda_A(A_c - A_{0c})^2$: $A_c$ is the area of a cell c, $A_{0c}$ its target area (minimum-energy area), and $\lambda_A$ an area compression modulus. This term enforces the cell area conservation. The pressure $p$ is defined and measured from $-2\lambda_A(A_c - A_{0c})$, averaged over all cells.

The theoretical value of the aggregate surface tension is calculated as: $\sigma = \gamma_{CM} - \gamma_{CC}/2$ (19). We checked (33) that for a liquid drop D, which in the cellular Potts model is represented by a single cell with constant interfacial tension $\gamma_{DM}$, the surface tension $\sigma$ is equal to $\gamma_{DM}$.

During one Monte Carlo time step, each pixel at a cell–cell interface is considered for update once, in a random order. If the pixel update diminishes the total aggregate energy, we accept it; and if the update increases the total energy by $\Delta\mathcal{E}$, we accept it with probability $P = \exp(-\Delta\mathcal{E}/\xi)$, where the "fluctuation allowance" $\xi$ leads to fluctuations of membrane positions (22).

Plates are used as force sensors, with a stiffness $k$ adapted to that of the aggregate. The potential energy of the plate surface is $\mathcal{E}_C = \frac{1}{2}k(\langle z\rangle - z_0)^2$, where $\langle z\rangle$ is the averaged vertical position of the plate interface, and $z_0$ the plate's zero-energy vertical position (33). The force $F$ on the plate is defined and measured as $F = k|\langle z\rangle - z_0|$.

To simulate a compression experiment, the zero-energy positions $z_0$ of the plates are approached by a step of 0.1 $h_{ag}$. Cell shapes, total force and aggregate radius are recorded during $10^5$ Monte Carlo steps (33). This is iterated until the aggregate height reaches 0.3 $h_{ag}$ (70% compression rate). In Fig. 3B and Fig. S4, parameters are: $\gamma_{CM} = 5.65 \times 10^5$, $\gamma_{CP} = 6.78 \times 10^5$, $\gamma_{MP} = 1.13 \times 10^5$, $\lambda_A = 1.0 \times 10^3$, $A_0 = 200$, $\xi = 4 \times 10^4$, $k = 2 \times 10^3$. The lattice size is $250 \times 800$ pixels, with 240 cells.

1. Holtfreter J (1944) Experimental studies on the development of the pronephros. *Rev Can Biol* 3:220–250.
2. Lin RZ, Chang HY (2008) Recent advances in three-dimensional multicellular spheroid culture for biomedical research. *Biotechnol J* 3:1172–1184.
3. Mgharbel A, Delanoë-Ayari H, Rieu J-P (2009) Measuring accurately liquid and tissue surface tension with a compression plate tensiometer. *HFSP J* 3:213–221.
4. Steinberg MS (2007) Differential adhesion in morphogenesis: A modern view. *Curr Opin Genet Dev* 17:281–286.
5. Wilson HV (1907) On some phenomena of coalescence and regeneration in sponges. *J Exp Zool* 5:245–258.
6. Steinberg MS (1963) Reconstruction of tissues by dissociated cells. Some morphogenetic tissue movements and the sorting out of embryonic cells may have a common explanation. *Science* 141:401–408.
7. Foty RA, Forgacs G, Pfleger CM, Steinberg MS (1994) Liquid properties of embryonic tissues: Measurement of interfacial tensions. *Phys Rev Lett* 72:2298–2301.
8. Norotte C, Marga F, Neagu A, Kosztin I, Forgacs G (2008) Experimental evaluation of apparent tissue surface tension based on the exact solution of the Laplace equation. *Europhys Lett* 81:R163–R165.
9. Foty RA, Pfleger CM, Forgacs G, Steinberg MS (1996) Surface tensions of embryonic tissues predict their mutual envelopment behavior. *Development* 122:1611–1620.
10. Gordon R, Goel NS, Steinberg MS, Wiseman LL (1972) A rheological mechanism sufficient to explain the kinetics of cell sorting. *J Theor Biol* 37:43–73.
11. Jakab K, Damon B, Marga F, Doaga O, Mironov V, Kosztin I, Markwald R, Forgacs G (2008) Relating cell and tissue mechanics: Implications and applications., *Dev Dyn* 237:2438–2449.
12. Mombach JCM, Robert D, Graner F, Gillet G, Thomas GL, Idiart M, Rieu JP (2005) Rounding of aggregates of biological cells: Experiments and simulations, *Physica A* 352:525–534.
13. Forgacs G, Foty RA, Shafrir Y, Steinberg MS (1998) Viscoelastic properties of living embryonic tissues: A quantitative study. *Biophys J* 74:2227–2234.
14. Brodland GW, Chen DI, Veldhuis JH (2006) A cell-based constitutive model for embryonic epithelia and other planar aggregates of biological cells. *Int J Plasticity* 22:965–995.
15. Malik WA, Prasad SC, Rajagopal KR, Preziosi L (2008) On the modeling of the viscoelastic response of embryonic tissues. *Math Mech Solids* 13:81–91.
16. Phillips HM, Steinberg MS (1978) Embryonic tissues as elasticoviscous liquids. I. Rapid and slow shape changes in centrifuged cell aggregates. *J Cell Sci* 30:1–20.
17. Phillips HM, Steinberg MS, Lipton BH (1977) Embryonic tissues as elasticoviscous liquids. II. Direct evidence for cell slippage in centrifuged aggregates. *Dev Biol* 59:124–134.
18. Yang J, Brodland GW (2009) Estimating interfacial tension from the shape histories of cells in compressed aggregates: A computational study. *Ann Biomed Eng* 37:1019–1027.
19. Graner F (1993) Can surface-adhesion drive cell-rearrangement. 1. Biological cell-sorting. *J Theor Biol* 164:455–476.
20. Weaire D, Rivier N (1984) Soap, cells and statistics—Random patterns in two dimensions. *Contemp Phys* 25:59–99.
21. Marmottant P, Raufaste C, Graner F (2008) Discrete rearranging disordered patterns, part II: 2D plasticity, elasticity and flow of a foam. *Eur Phys J E* 25:371–384.
22. Mombach JC, Glazier JA, Raphael RC, Zajac M (1995) Quantitative comparison between differential adhesion models and cell sorting in the presence and absence of fluctuations. *Phys Rev Lett* 75:2244–2247.
23. Beysens DA, Forgacs G, Glazier JA (2000) Cell sorting is analogous to phase ordering in fluids. *Proc Natl Acad Sci USA* 97:9467–9471.
24. Rieu JP, Upadhyaya A, Glazier JA, Ouchi NB, Sawada Y (2000) Diffusion and deformations of single hydra cells in cellular aggregates. *Biophys J* 79:1903–1914.
25. Mombach JC, Glazier JA (1996) Single cell motion in aggregates of embryonic cells. *Phys Rev Lett* 76:3032–3035.
26. Eyring H (1935) The activated complex in chemical reactions. *J Chem Phys* 3:107–115.
27. Krieg M, et al. (2008) Tensile forces govern germ-layer organization in zebrafish. *Nat Cell Biol* 10:429–436.
28. Yamada S, Wirtz D, Kuo SC (2000) Mechanics of living cells measured by laser tracking microrheology. *Biophys J* 78:1736–1747.
29. Watanabe N, Mitchison TJ (2002) Single-molecule speckle analysis of actin filament turnover in lamellipodia. *Science* 295:1083–1086.
30. Nagafuchi A, Shirayoshi Y, Okazaki K, Yasuda K, Takeichi M (1987) Transformation of cell adhesion properties by exogenously introduced E-cadherin cDNA. *Nature* 329:341–343.
31. Graner F, Glazier JA (1992) Simulation of biological cell sorting using a two-dimensional extended Potts model. *Phys Rev Lett* 69:2013–2016.
32. Marée AFM, Grieneisen VA, Hogeweg P (2007) The cellular Potts model and biophysical properties of cells, tissues and morphogenesis. *Single Cell Based Models in Biology and Medicine*, eds Anderson ARA, Chaplain MAJ, Rejniak KA (Birkhäuser, Basel), pp 107–136.
33. Käfer, J (2008) From cells to tissues: Physical modelling of the collective behaviour of embryonic cells. PhD thesis, University Joseph Fourier–Grenoble I, available at http://tel.archives-ouvertes.fr/tel-00346418/fr/.

BIOPHYSICS AND
COMPUTATIONAL BIOLOGY

PHYSICS